

# PARAMETER AND DEPOSITION STRATEGY ANALYSIS FOR WAAM PROCESSING OF AISI 410

I. Pires<sup>1\*</sup>, E. G. Assunção<sup>2</sup>, M. C. Florescu<sup>3</sup>,  
I. D. Savu<sup>3</sup>, M. C. Criveanu<sup>3</sup>, D. Klobčar<sup>4</sup>

<sup>1</sup> Universidade de Lisboa, IDMEC, Instituto Superior Técnico, Av. Rovisco Pais, 1049-001 Lisbon, Portugal

<sup>2</sup> European Federation for Welding, Joining and Cutting, Oeiras, Portugal

<sup>3</sup> University of Craiova, Faculty of Mechanics, Craiova, Romania

<sup>4</sup> University of Ljubljana, Faculty of Mechanical Engineering, Ljubljana, Slovenia

\*Corresponding author's e-mail address: inespres@tecnico.ulisboa.pt

## ABSTRACT

*Wire + Arc Additive Manufacturing (WAAM®) is an additive manufacturing (AM) process capable of producing near net shape parts while reducing costs and thus gathering increased attention from researchers and manufacturers. Although a significant amount of work has already been published relating to the WAAM processing of stainless steels, it was mainly focused on austenitic stainless steels, with martensitic grades still lacking investigation. AISI 410 is a martensitic stainless steel that, due to its high hardness, demonstrates high wear resistance, being used in parts requiring high resistance to abrasion. Processing this material by WAAM allows for the creation of near net shape parts, leading to a reduction in machining, while at the same time allowing the creation of complex geometries which would be difficult, or outright impossible to obtain otherwise. In this work the effects of different processing parameters on WAAM processed AISI 410 steel, using Cold Metal Transfer (CMT) welding equipment, were investigated, as well as different deposition strategies for the fabrication of a test artifact using an AM software. It was demonstrated that it is possible to process AISI 410 steel by WAAM using an AM software to define deposition strategies and parameters based on the part design and previous experimental trials. The goal to deposit a complex part with high hardness and tensile strength, especially attractive properties to parts requiring high resistance to wear was achieved.*

**KEYWORDS:** Wire and Arc Additive Manufacturing, DED+Arc, AISI 410, martensitic stainless steel, CMT, deposition strategy

## 1. INTRODUCTION

In an attempt to reduce costs and material waste, Additive Manufacturing (AM) processes have witnessed an increase in research as of late. Considered little more than a novelty when it first emerged, THE AM processing of materials has begun to find its place in the industrial environment, promising personalized items at no increased cost, shortening of supply chains and reducing the material waste [1],[2].

Being one of the cornerstones of engineering applications, AM techniques for the processing of metals have been and are being researched as of now, seeking to take advantage of the benefits brought by this technology. Among these techniques, Directed Energy Deposition (DED), and, more specifically Wire and Arc Additive Manufacturing (WAAM), is one of the most promising for an industrial environment. Being an arc-based process and using metallic wire as

feedstock, this process builds upon vastly researched welding processes to build increasingly complex parts, while enjoying high deposition rates, reduced material waste and ease of access to the process itself [3].

WAAM is being increasingly researched and the range of materials that can be used by applying this technology is continuously expanding, increasing its field of applications. Therefore, there is a great interest to research this subject and contributing to the advancement of the manufacturing industry. Although significant research on the use of stainless steel in WAAM applications has already been published, it is mainly focused on austenitic stainless steels, such as 304L [4], 308LSi [5] and 316L [6], with research in martensitic stainless steels still lacking. Due to the high hardness values, characteristic of this microstructure, parts created with this grade of steels show a high resistance to wear, [7], which can make machining more difficult to execute.

Being an additive manufacturing process, WAAM allows for the construction of a wide range of complex geometries, without the constraints associated with traditional manufacturing techniques and dismissing the need of specific tools for different geometries. In addition, WAAM allows for the creation of near net shape parts, reducing the amount of machining necessary to obtain a final form when compared with traditional manufacturing techniques. Nevertheless, manually programming the deposition path for these complex geometries presents itself as an extremely time-consuming process, thus creating the need of a computer software to address this issue.

From the available welding processes currently used in WAAM, CMT is gaining interest among researchers. Being a variant of GMAW this process not only produces weld beads with good quality, stable arc, a lower heat input than other DED processes and nearly spatter-free depositions [8] but it is also easy to operate and combine with a robotic system [9]. P.M Cerqueira et al. [10]. tested different DED-arc processes concluded that for steel the most favourable process conditions are the ones provided by CMT, with homogeneous hardness profiles, good mechanical strengths, without decohesion in external layer; CMT Continuous gave optimal due to the better mechanical properties in comparison with single CMT. Stinson et al. [11] also study GMAW derived process: MIG and CMT. Characterization of parameter sets revealed relationships between torch travel speeds, wire feed speeds and the specimen properties and proportions. Differences were observed in the cross-sectional bead geometry and deposition rates when comparing MIG and CMT samples though the influence of process mode on mechanical properties was less significant compared to process parameter selection.

Liu et al summarised the research developments of WAAM, which included suitable metal materials and processing technology, deposition strategy optimization, slicing and path planning algorithm, multi-sensor monitoring and intelligent control, and the large complex metal components manufacturing technology [12].

Based on the advantage of the characteristics of WAAM and martensitic stainless steels, the research was focused on the optimization of CMT operating parameters and deposition strategies to produce a test artifact by WAAM, using martensitic stainless steel, AISI 410, and programming the deposition path through an AM software. Due to the typical properties of the martensitic stainless steel, it is expected that the material used in the work to relieve a high wear resistance. Although no study on WAAM processed AISI 410 was found, a study on multipass welding for this material was carried out by Amrei et al. [13]. A complex and heterogeneous microstructure was observed, with several regions affected by adjacent weld beads, which led to a variation of hardness values across the weld beads, with values ranging from 340 HV to 400 HV.

Wang et al. investigated the properties of AISI H13 steel, discovering that, for thin-walled structures, Vickers hardness was kept uniform across the height of the samples, assuming values between 300 and 360 HV [14]. For the same steel Ou et al developed, tested and used a three-dimensional heat transfer and fluid flow model of WAAM to calculate temperature and velocity fields, deposit shape and size, cooling rates and solidification parameters [15].

Xu et al. investigated the deposition of a MARVAL 18S maraging steel by WAAM. It was observed that a significant difference in hardness, from 330 HV at the bottom to 430 HV at the top, was found along the height of the part, due to the aging effect from each successive deposition. This difference was eliminated after aging the part and the hardness value increased, reaching 550 HV, suggesting that incorporating aging treatment could be very beneficial to the production of wear-resistant steel parts. As for tensile properties, a UTS of 1165 MPa and an elongation of 13,7% were observed [16].

Martina et al. investigated the deposition of martensitic stainless steel 17-4 PH, evaluating its microstructure and mechanical properties after deposition. They observed a dendritic microstructure with interdendritic  $\delta$ -ferrite in a lath martensitic matrix. It was also observed that the grain size increased for higher heat inputs, leading to a decrease in hardness, which was found to be between 340 HV and 348 HV, with no significant changes across the tested samples made with different process parameters [17].

One of the most evident issues when depositing single wall is the starting and ending height that show considerable difference from the middle section. This happens when the start and end point is the same for every layer, where excessive heat sink at the initial deposition point causes a lack of weld penetration, creating an increase in layer height. On the opposite side at the final deposition point, low heat dissipation, causes a drop in layer height [18]. This error will accumulate throughout the building process, creating a considerably large difference between both edges. Two methods are currently employed to overcome these differences. One of them is to control the process parameters, namely the current and travel speed of the torch, increasing them when beginning the deposition and reducing them when finishing it [19]. The other method employs a "zig-zag" motion of the torch where the start and end point of deposition changes with every layer [20]. This method also solves the problem satisfactorily, but it can also result in high residual stresses at the wall boundaries, due to thermal accumulation in certain zones [18].

Understanding the interdependency between the weld bead geometry and the process parameters, has a significant importance in obtaining parts free of defects. Researchers have tried to correlate welding parameters and bead geometry by regression analysis [21], artificial neural networks or combinations of these two techniques [22]. Xiong et al. have

determined that the optimal model of bead profile was dependent of the ratio between wire feed speed and travel speed of the torch, by comparing measured weld bead deposited with different welding parameters with three bead profile models [23]. In [24], it was analysed the effect of three different deposition strategies on surface waviness and porosity in steel (oscillation, parallel and weaving). In this study Xu et al. determined that employing a weaving strategy not only resulted in a better surface finish, with a flatter top, which requires less machining after deposition, but also led to a decrease in porosity in welds.

To minimize the number of starts and stops of the torch and welds intersections, decomposition of CAD models has been studied and carried out. D. Ding et al. [25] decomposed layers in polygons, filling each area and generating a closed loop toolpath, where Kao and Prinz [26] divided the geometry of a slice plane in a set of bisector segments. When these segments connect at more than two points they become branch points, with the deposition's paths being generated around the segments connected by them.

**Table 1.** Chemical composition of OK Autrod 410NiMo steel in Wt%

Element	C	Mn	Si	Ni	Cr	Mo	Cu
Wt %	0.02	0.5	0.4	4.2	12.4	0.6	0.1

## 2.2. Description of the Deposition Process

The deposition work was performed using a 6-axis KUKA robot coupled with a Fronius CMT welding machine: Model: TPS 4000 CMT Wire feeder: VR 7000 CMT Maximum Current Intensity: 400 A. The shielding gas used for the deposition work was ARCAL Chrome, a mixture of Ar+2%CO<sub>2</sub>-ISO 14175-M12-ArC-2. The substrates were clamped to a steel table. This setup is presented in Figure 1.

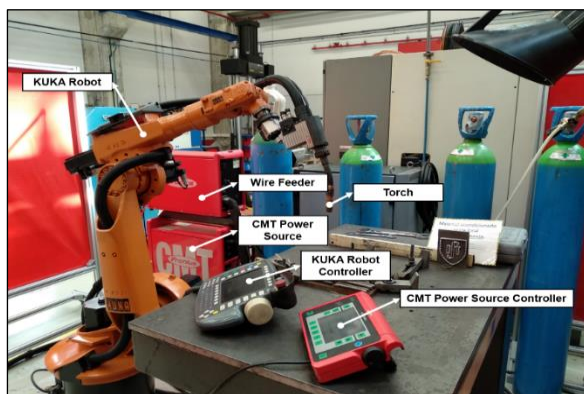


**Fig. 1** Deposition work setup

## 2.3. CMT Operating Parameters

Samples were deposited using a CMT welding equipment and various process parameters.

## 2. EXPERIMENTAL PROCEDURE

### 2.1. Materials

The material used for this work was a martensitic stainless steel, OK Autrod 410NiMo (Table 1). It was supplied in wire form, by ESAB, with a diameter of 1.2 mm, in a 15 Kg spool. Like all martensitic steels, AISI 410 possesses high corrosion resistance, high strength and high toughness.

Due to its low carbon content of 0.02%, it is considered a supermartensitic stainless steel and it is used in various industries for the fabrication of essential parts, such as parts for computer hard drives, plastic moulds, screws, valves, shafts, bearings and pipelines as an alternative to austenitic and duplex stainless steels. Table 1 provides the chemical composition of the AISI 410 wire. The substrate material was a low carbon steel, prepared as plate with 250 x 200 x 15 [mm] dimensions.

In order to determine the effect that parameters have on the quality of the deposition, only one parameter was varied the others been maintained constant. The Shielding Gas Flow Rate (SGFR) and Contact Tip to Work Distance (CTWD) were kept constant at 18 L/min and 15 mm, respectively, throughout all depositions.

The Wire Feed Speed (WFS) was modified in a range of values that the welding machine controller allowed. The other modified parameter was the Travel Speed (TS) of the torch, computed from a range of ratios WFS/TS. This ratio provides an indication on the volume of deposited material per unit of length, with higher ratios indicating higher amounts of material. This ratio provides the simplest relationship between processing parameters and bead shape. It is also a key factor for wall dimensions, with increasing ratios providing increased wall width, layer height and surface waviness [27], allowing to determine the combination of process parameters that produce a quality weld and adequate material deposition.

With the selected CMT waveform, which depend on the material and shielding gas selected, the WFS range was 3 – 6 m/min. Based on a few initial trials, two sets of experiments were performed in order to determine CMT operating parameters, one with a linear deposition path (see Fig. 2a) and another with an oscillating deposition path (see Fig. 2b). The parameters used for linear and oscillating deposition paths are presented in Table 2 and Table 3, respectively.

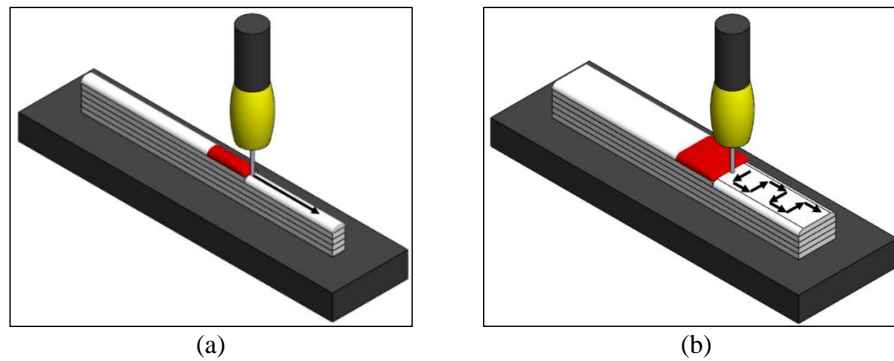


**Fig. 2.** Schematic representation of deposition paths: a) linear deposition path, b) oscillating deposition path [28]

**Table 2.** Linear deposition path CMT parameters

Case	WFS [m/min]	TS [m/min]	WFS/TS
L1	3	0.12	25
L2		0.15	20
L3		0.20	15
L4		0.30	10
L5	4	0.16	25
L6		0.20	20
L7		0.27	15
L8		0.40	10
L9	5	0.20	25
L10		0.25	20
L11		0.33	15
L12		0.50	10
L13	6	0.24	25
L14		0.30	20
L15		0.40	15
L16		0.60	10

**Table 3.** Oscillating deposition path CMT parameters

Case	WFS [m/min]	TS [m/min]	WFS/TS
O1	3	0.30	10
O2		0.20	15
O3		0.15	20
O4	4	0.40	10
O5		0.27	15
O6		0.20	20
O7	5	0.50	10
O8		0.33	15
O9	6	0.60	10

## 2.4. Material Characterization

In order to assess the deposited material behaviour, material characterization tests were carried out. Hardness tests were performed on the linearly deposited samples. Indentations were performed with a Struers Duramin. Ten indentations were performed, under a load of 5 N for 10 s, spaced 1 mm between them, along the height of the samples.

Metallographic analysis and tensile tests were also performed. The samples for metallographic analysis were grounded using abrasive papers, with grit ranging from 80 to 1000, polished, and etched with Vilella reagent by immersion to reveal the microstructure.

Tensile tests were made with an INSTRON Universal Testing Machine with a 200 kN cell. The elongation was measured by an extensometer placed on tensile specimens. Tests were performed with a load speed of 1 kN/min, following a ramp function, until reaching yield stress, and afterwards a constant speed of 5 mm/min until finishing the test. The specimens were manufactured according to the *ISO 6892-1:2019 Metallic materials — Tensile testing — Part 1: Method of test at room temperature*.

## 2.5. Test Artifact

A test artifact was designed in order to validate the parameters obtained in the parametrization stage and the deposition strategies that were generated, using an AM software. This test artifact, presented in figure 3, was created taking into account some guidelines for the design of parts to be manufactured by WAAM.

The first aspect to be considered was the width of the walls. With WAAM having a relatively large minimum feature size, usually larger than 2 mm, complex geometries with exceedingly small dimensions are impossible to obtain without post machining, which depending on the geometry itself could prove difficult or outright impossible. In addition, very thin walls could distort during deposition and their use should be avoided when employing this manufacturing process. Wall width should then be defined accordingly to the bead dimensions that are deposited with the set of parameters that are employed. On the other hand, although a minimum part size exists, a maximum size is only limited by the dimensions of the work environment and robotic system reach [28].

Another aspect to consider is the intersections between the outer and inner sections. Intersecting segments require a sufficient amount of overlap between them, in order to avoid defects such as lack of fusion between them. However, if this overlap is excessive, it can lead to defects such as humping, due

to the accumulation of successive weld beads. This humping defect also leads to a depression on the opposite side of the crossing paths, leading to an unstable arc when the torch moves over this area [29]. These defects will aggravate as more layers are deposited, and could lead to collisions between the torch and the part. Therefore, a strategy must be defined where sufficient overlap is introduced to avoid lack of fusion between segments without introducing humping. When manufacturing a part, by any process, care should be taken to avoid introducing sharp corners in its geometry. Not only they act as stress raisers, they are also impossible to machine if they are internal. Although external sharp corners can be obtained by WAAM, it is advisable to avoid them, since they

require a sudden change in deposition direction forcing a stop/start movement of the torch and, as mentioned before, act as stress raisers. The introduction of a radius, for both internal and external corners is advantageous for several reasons. They allow for post machining and avoid the introduction of a stress raiser geometry. Specific to WAAM, they also allow for an increase in deposition path fluidity, reducing the stop/start movements of the torch, and allow for more material to be introduced in the corner of the part, leading to a reduction of voids and porosities. This increase on the amount of material introduced in the corner also allows to obtain a sharp edge by machining, should it be required [28], [30].

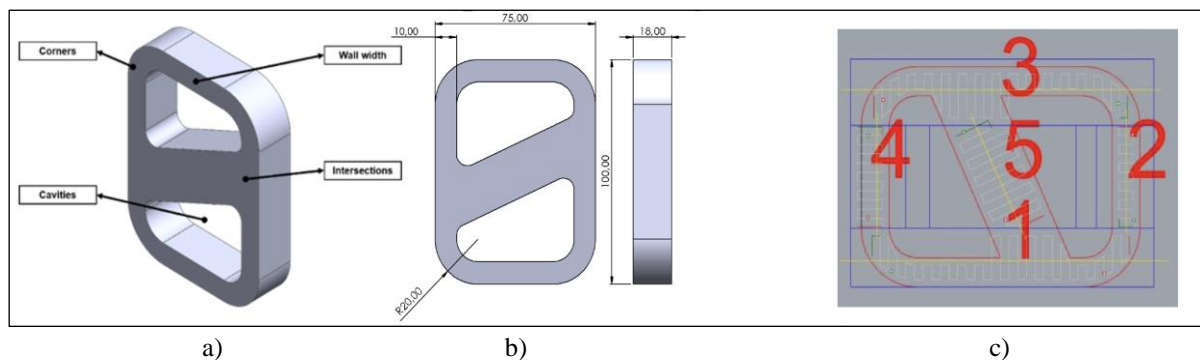


**Fig. 3.** Test artifact: a) shape; b) dimensions; c) example of path planner using WAAMMAT programme

Heat accumulation is also a key factor that influences the geometrical accuracy, defects during deposition, microstructure, and material properties of deposited parts. Controlling the interlayer temperature is essential to ensure that defects introduced by heat accumulation do not manifest. At an initial stage, heat generated by the process is conducted to the substrate, kept at a relatively cool temperature when compared to the deposited layer. As building height increases this effect is reduced by a magnitude which is dependent on the material thermal conductivity, leading to a shift on the heat transfer mode from conduction to convection and radiation to the surrounding atmosphere. Nevertheless, these heat transfer modes are less effective than conduction through the substrate, leading to an increase in heat accumulation and interlayer cooling waiting time [31].

The introduction of cavities allows for an increased surface area when compared to a massive block, allowing for a more efficient cooling of the artifact during its deposition, mitigating the effects of heat accumulation.

### 3. RESULTS AND DISCUSSION

#### 3.1. CMT Operating Parameters for Linear Deposition

For the first study, sixteen linear depositions were carried out, with six layers each. A visual inspection of

the depositions was made, which allowed to define the acceptable, when glaring defects in the bead geometry, such as humps or discontinuities, were not present, and unacceptable depositions, otherwise.

These depositions were also measured with a set of callipers. Five measurements were taken in order to calculate average width and height, which allowed to calculate the percentage of deviation from the average for each of the trials. Quantifying how much the measured values deviate from the average allowed to determine which trials produced the most regular depositions. It should be noted that trials L1 and L4 present slight irregularities in their extremities, not enough to be considered unacceptable.

The resulting depositions for each trial are presented in Fig. 4a, the trial classifications based on visual inspection are presented in Fig. 4b and the width and height deviations are shown in Fig. 4c. Fig. 4c shows that a WFS of 3 m/min produces depositions with the largest percentage of deviation values, with decreased values observed when WFS is increased.

Trial L5, with a WFS of 4 m/min and a WFS/TS ratio of 25, presents the lowest value for percentage of deviation in both height and width, being selected as reference to be used in the linear path depositions. Besides the aforementioned value of percentage of deviation, the measurement of these depositions, presented in figure 5, also allowed to define the stepover parameter for the oscillating deposition paths, as 66% of the bead width, as already verified [28].

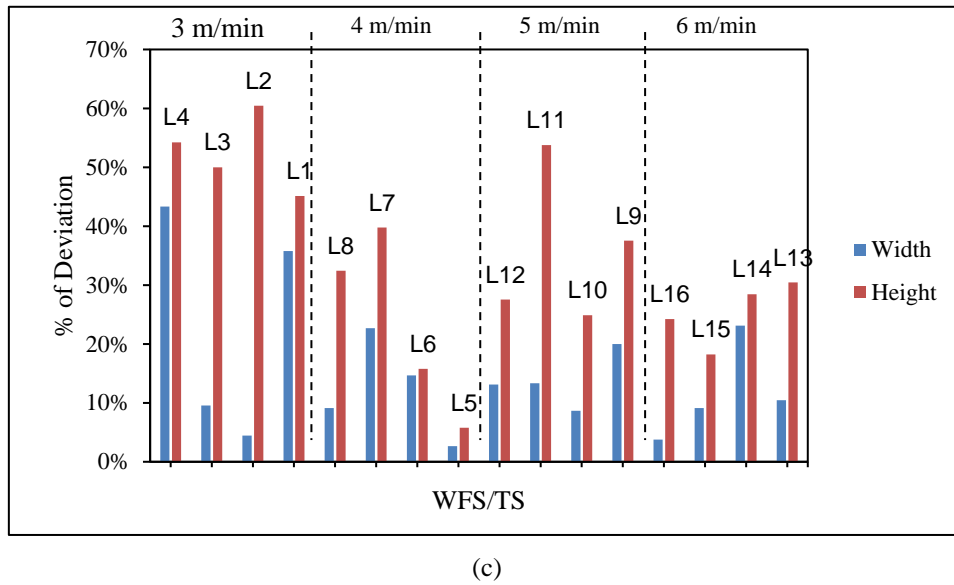
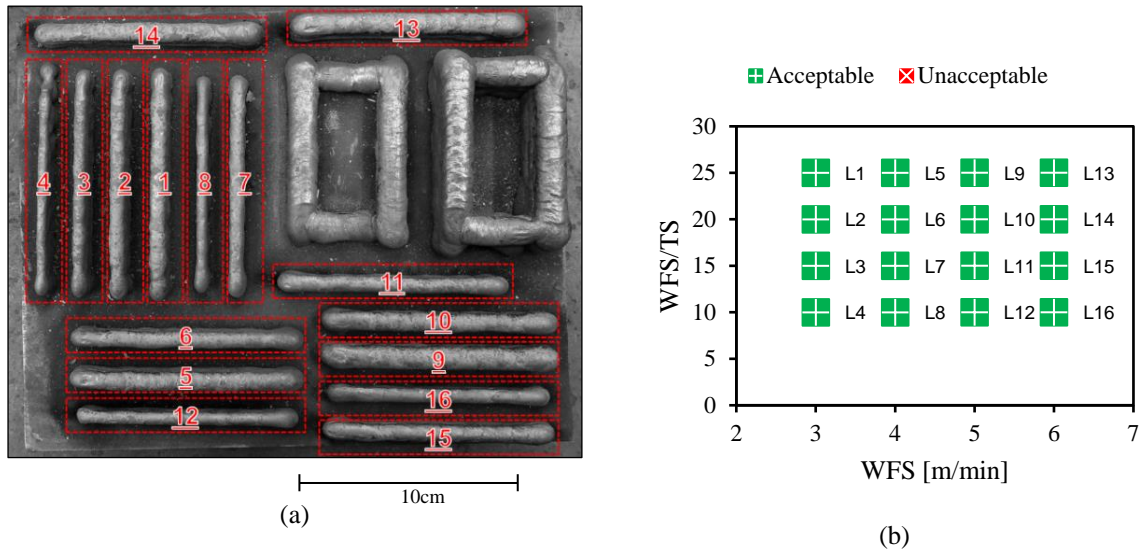


Fig. 4. Linear deposition: a) samples; b) visual inspections results; c) average dimension of each deposition

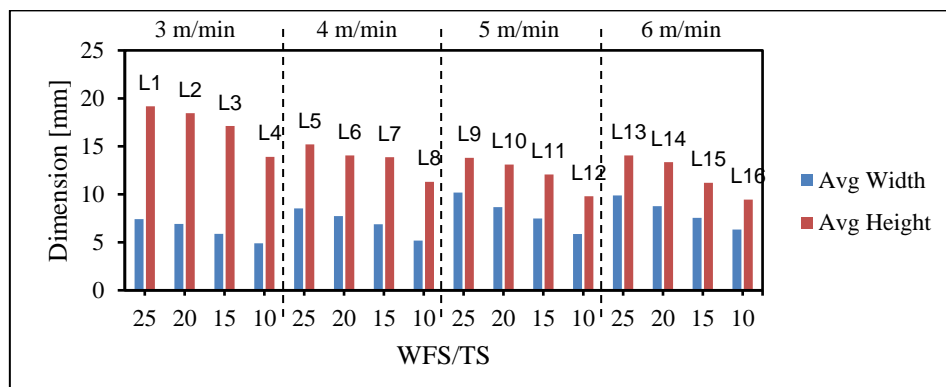


Fig. 5. Average dimension of each layer made by linear deposition

In addition, it can be seen that the width of the deposits, for the same value of WFS, increases with the WFS/TS ratio. This is an expected behaviour, since

increasing WFS/TS means reducing the TS of the torch, introducing more material into the melt pool. For the same reason, increasing the WFS also led to larger

bead width for the same WFS/TS ratio, although in a smaller magnitude. The average height of each bead increases when the WFS/TS ratio is increased and the WFS is kept constant, as expected, also due to more material being deposited per unit of length which allows for the height to build up at a faster rate.

### 3.2. Hardness Testing

Figure 6 presents the Vickers hardness values in case of AISI 410 linearly deposited samples that showed the lowest percentage of deviation in each WFS bracket, the indentation points along the sample and the evolution of hardness values for trial L5. In figure 6a it

can be seen that, for the tested trials, the average values for Vickers Hardness are between 372 HV and 412 HV. These values are lower than the 450 HV found in literature for the “as welded” condition for a single bead [32], but in line with the values obtained in a multipass welding study for this material, carried out by Amrei et al. [34]. This lower hardness is related with the constant reheating of the sample as new layers are added, leading to coarser grain size. Figure 6b illustrates the location of indentations and figure 6c shows the hardness evolution for trial L5, revealing the hardness increasing close to the substrate until an approximately constant value is reached.

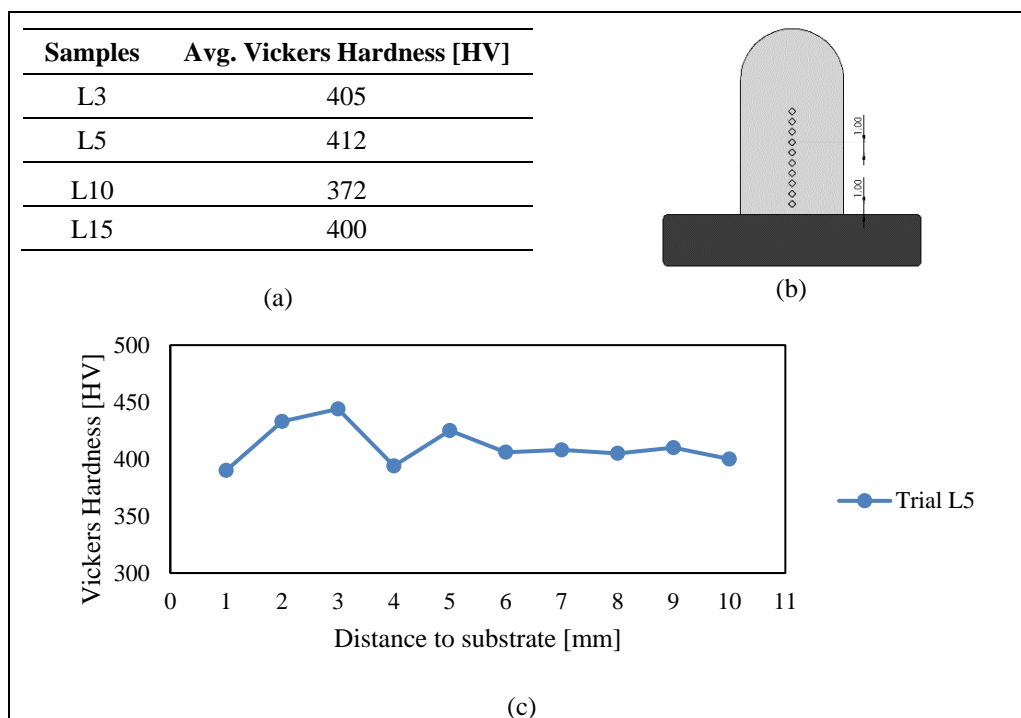


Fig. 6. Hardness testing results: a) average HV values; b) indentations; c) HV values for L5 sample

### 3.3. CMT Operating Parameters for Oscillating Deposition

A second set of trials was carried out with the purpose of determining the best parameters that would allow for regular depositions when employing an oscillation strategy. Nine depositions were carried out, following an oscillation path, with six layers each. For the oscillating depositions trials O1, O4, O5 and O7 were considered acceptable.

Following the same criteria referred in 1.1, each trial was visually inspected and classified accordingly. Each trial was also measured in order to calculate the percentage of deviation from the average, following

the same methodology as for the linear trials. The resulting depositions are presented in Fig. 7a, the classifications based on visual inspection are presented in Fig. 7b and calculated percentages of deviation are presented in Fig. 7c. Fig. 7c shows that trial O1, with a WFS of 3 m/min and WFS/TS ratio of 10, showed the lowest combination for percentage of deviation, making the parameters used in this trial the reference when depositing with an oscillating path.

These values for WFS and WFS/TS ratio produced beads with high percentages of deviation in linear deposition trials, showing that the parameterization work has to be performed for different deposition path patterns.

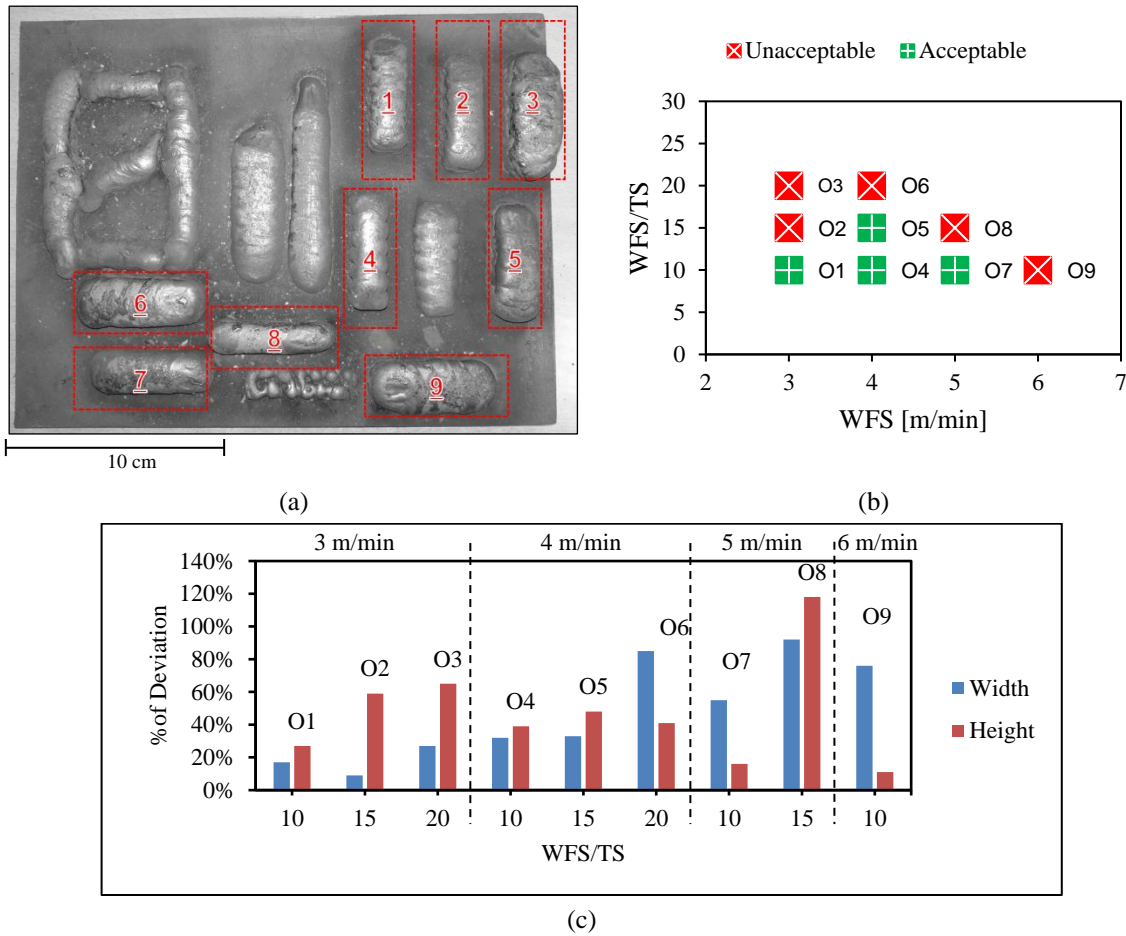


Fig. 7. Oscillating deposition: a) samples; b) visual inspection results, c) deviation vs. WFS/TS ration

**3.4. Deposition strategy: Application to the test artifact**

To identify the best strategy deposition to be applied in the designed test artifact, an AM software was used in combination with the parameters defined for trials L5 and O1, for depositing linear and oscillating paths,

respectively. Each test artifact was made depositing six layers. Two strategies were defined initially. In the first one the outer section comprised of a linear deposition following the contour of the test artifact while the inner section was deposited following an oscillation path. For the second one, an oscillation path was employed in both sections of the test artifact. These strategies and resulting depositions are presented in Fig. 8.

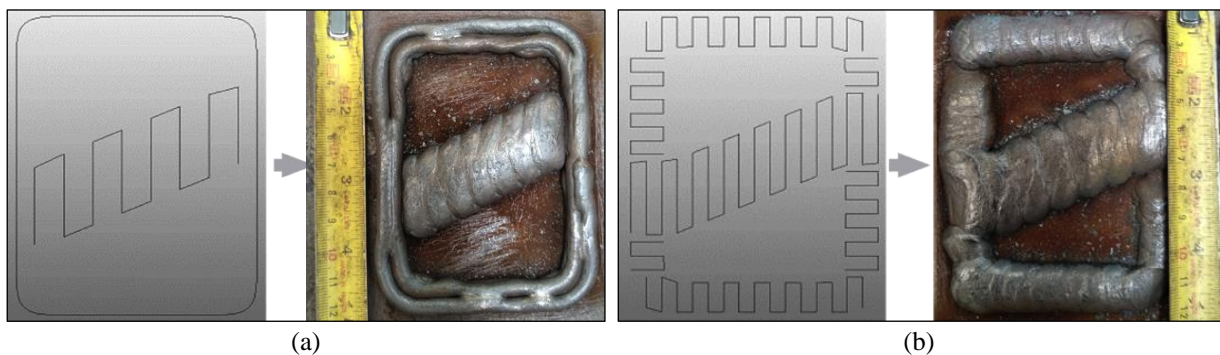


Fig. 8. Deposition strategies for test artifact: a) linear + oscillating strategy; b) oscillating strategy

Although the general shape of the part was obtained, some issues can be observed. A lack of connection is visible in the beads that compose the

outer section, meaning that the stepover parameter was not properly selected. In addition, a lack of connection between outer and inner section is also observed. As

for the second strategy, like in the previous one, it is also observed a lack of connection between segments, as well as an irregular geometry, with deviations in segment dimension and material buildup near the corners, suggesting that the parameters and deposition path require further optimization. Before attempting to further optimize parameters, another software was used to generate the deposition paths. This software allowed for a finer control of part segmentation, simplifying the process of solving segment connectivity issues. Oscillation paths were used with this software, therefore reference parameters from trial O1 were used as reference for depositing the test artifact. The first defined strategy (see Fig. 9a), saw a reduction in the number of segments of the deposition path, which means a reduction in the amount of stop/start

movements of the torch. In addition, the path curves slightly near the corners, following the contour of the test artifact, instead of abruptly changing directions like in the oscillation path created with the previous software. After defining the procedure for the test part deposition, new tests were made increasing the height of the initial version of the test artifact. This analysis was made in order to determine if the increase in number of layers introduced any defects which did not occur with a reduced number of layers. In this context thirty-four layers were deposited and the observed deposition showed a defect close to the halfway point, in layer fifteen, which was not present before. The depositions made using these last strategies and the aforementioned defect are presented in Fig. 9.

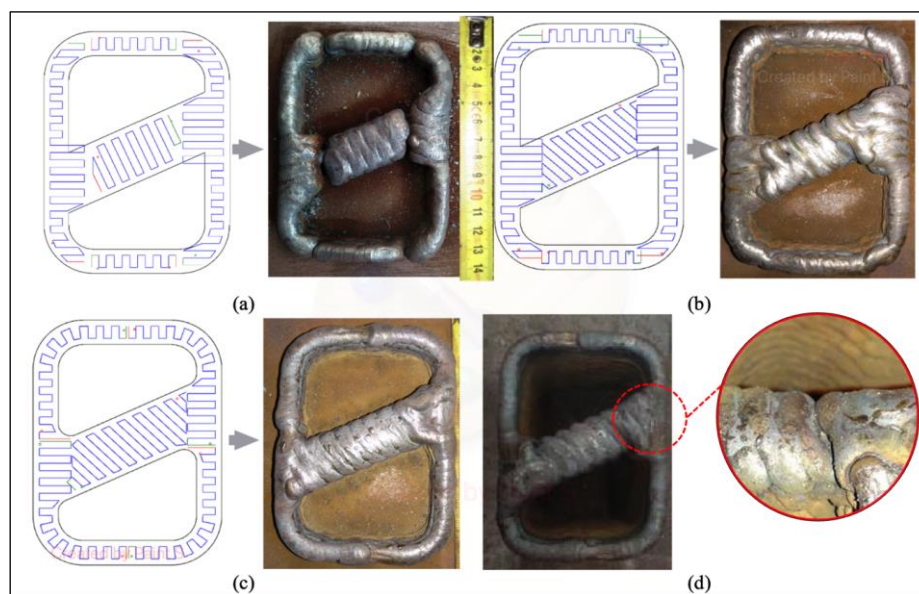


**Fig. 9.** Deposition strategies and samples achieved: a first strategy, b second strategy with increased overlap, c third strategy with improved deposition path fluidity, d detail of the defect introduced with increase in the number of layers in layer 15

In the first strategy, a lack of connectivity between segments, the material buildup in the corners and the areas where the outer section intersects the inner section can still be observed. To overcome these issues the deposition path was adjusted in the second strategy, increasing the overlap between segments. It can be observed that segment connectivity is now complete, although this approach led to an increase in material accumulation in the corners of the part, contributing to their irregularity.

In order to address the issues still present, the deposition path was adjusted once more, moving the starting point of the weld in every segment that composed the outer layer away from the corners, increasing the fluidity of the deposition path by eliminating a stop/start movement of the torch in these areas where the direction of deposition changed. Segment connectivity is now complete and excess of material in the corners is considerably reduced, making

this strategy the one used as reference for the deposition of the test artifact with increased height. It would be expected that the use of a single continuous oscillating deposition path for the outer layer would provide even better results, however, due to software limitations, this section had to be divided in four segments.

The extended version of the test artifact had its height increased to 100 mm. During deposition it was observed that the corners and linear segments of the part retained their regularity, the connection between segments was complete, without visible gaps between them. Nevertheless, the increase of the number of layers caused the defect present in figure 9d. Like stated before this defect was introduced indirectly by the increase in height, since the additional thermal cycles created by it led to lower thermal gradients and, consequently, higher heat accumulation. This heat accumulation increased the solidification time of the

metal, which led to material flowing out of place. The reason why this defect is not present in other areas of the part is that a higher amount of material is deposited in this section. To solve this defect, the time between layers was increased, to increase the cooling time.

In order to control the temperature between each successive layer deposition a Hanna HI 935005 thermocouple thermometer was used. To ensure that the temperature was being carefully measured a comparison was made using a commercial camera Fluke TiS400 ® that was positioned on a tripod. The infrared image sequence was acquired through an infrared sensor with 320 x 240 resolution with the frequency variation of 9 Hz. The camera was used to

record the whole process of manufacturing. Each layer was recorded and the SmartView® software was used for analysis and reporting the infrared image. The interlayer temperature was maintained around 200 °C. In figure 10, it is presented the sample carried out after depositing 34 layers. During deposition it was observed that the corners and linear segments of the part retained their regularity, the connection between segments was complete, without visible gaps between them. Nevertheless, the increase of the number of layers causes the accumulation of excess of buildup material in the Z direction that was not present before. It is also visible that controlling the interlayer temperature corrected the defect present before.

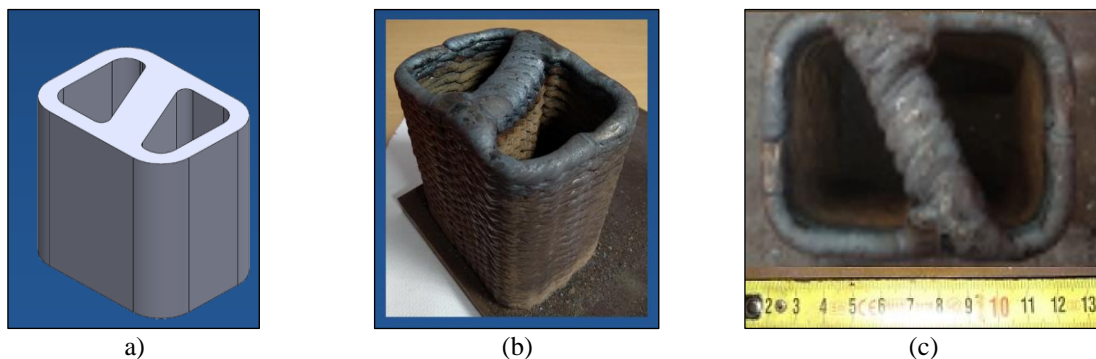


**Fig. 10.** Test artifact: a) CAD image; b) printed perspective view; c) printed top view

### 3.5. Microstructure Analysis

In the figure 11 it can be observed a section of the deposited test artifact with 100 mm in height, with no common welding defects being detected, such as cracks, porosity or lack of fusion. Although the deposit metal being a martensitic grade steel, AISI 410, prone to cold cracking, that can of metallurgical problem was not also detected on the analysed samples. This might be due to interlayer temperatures and the successive layers that are added, acting like a post heat treatment. Also, it can be observed the gradient of macrostructure along the building direction, where it is observed a well-known grain morphology of AM parts, a columnar region aligned along the buildup direction, following the heat flow direction towards the surface of each bead. The microstructure in different segments of the wall can also be observed, with a martensitic structure present along the entire length of the wall, which becomes with a progressively coarser grain size, consequence of the successive reheating of the wall during deposition.

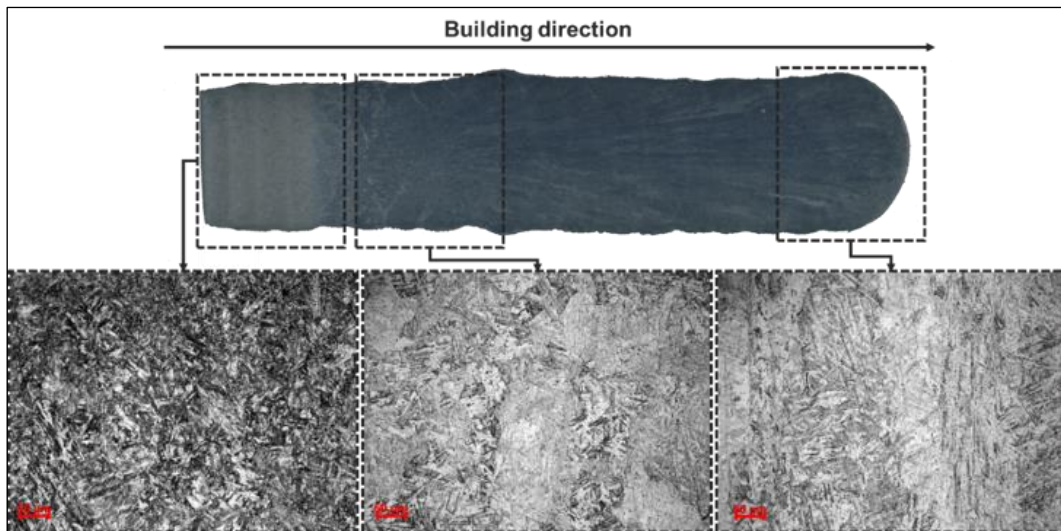
In the figure 12 fully martensitic microstructure is visible, with a calculated percentage of 0.91% carbon equivalent, expecting to achieve a mixture of lath and plate martensite. Retained austenite can also be noticed, which is softer than martensite, and is leading to a decrease in hardness and an increase in ductility.

Figure 13 shows a mixture of tempered and freshly formed martensite. The martensite present in these

section of the sample shows a finer microstructure than the one present in Figure 12. Carbides can also be observed, showing as small round dots. Grain size also shows an increase in dimension due to the additional thermal cycles, with a further increase expected closer to the top of the sample.

In the figure 14, it can be observed regions with column shaped microstructure and fine martensite microstructures. This column shaped microstructure follows the direction of the heat flow towards the top of the sample. These were probably austenite columnar grains that were not modified in a significant manner by the martensitic transformation during cooling. Another possible explanation is that, in some regions, the heat of the deposition of new layers raised the temperature to the austenitic region and, as they cooled and transformed back into fresh martensite, the columnar microstructure remained [26-29]. Carbides are also visible in these micrographs. Like expected, successive thermal cycles increased grain size even further when compared with the previous analysed sections.

The direction of dendrite growth is primarily determined by the heat flow in the material. In CMT, the heat is typically applied from the welding torch to the previously deposited layers. As a result, dendrites tend to grow perpendicular to the deposition direction, which will lead to different properties in different directions.



**Fig. 11.** Metallographic analysis of sample wall section

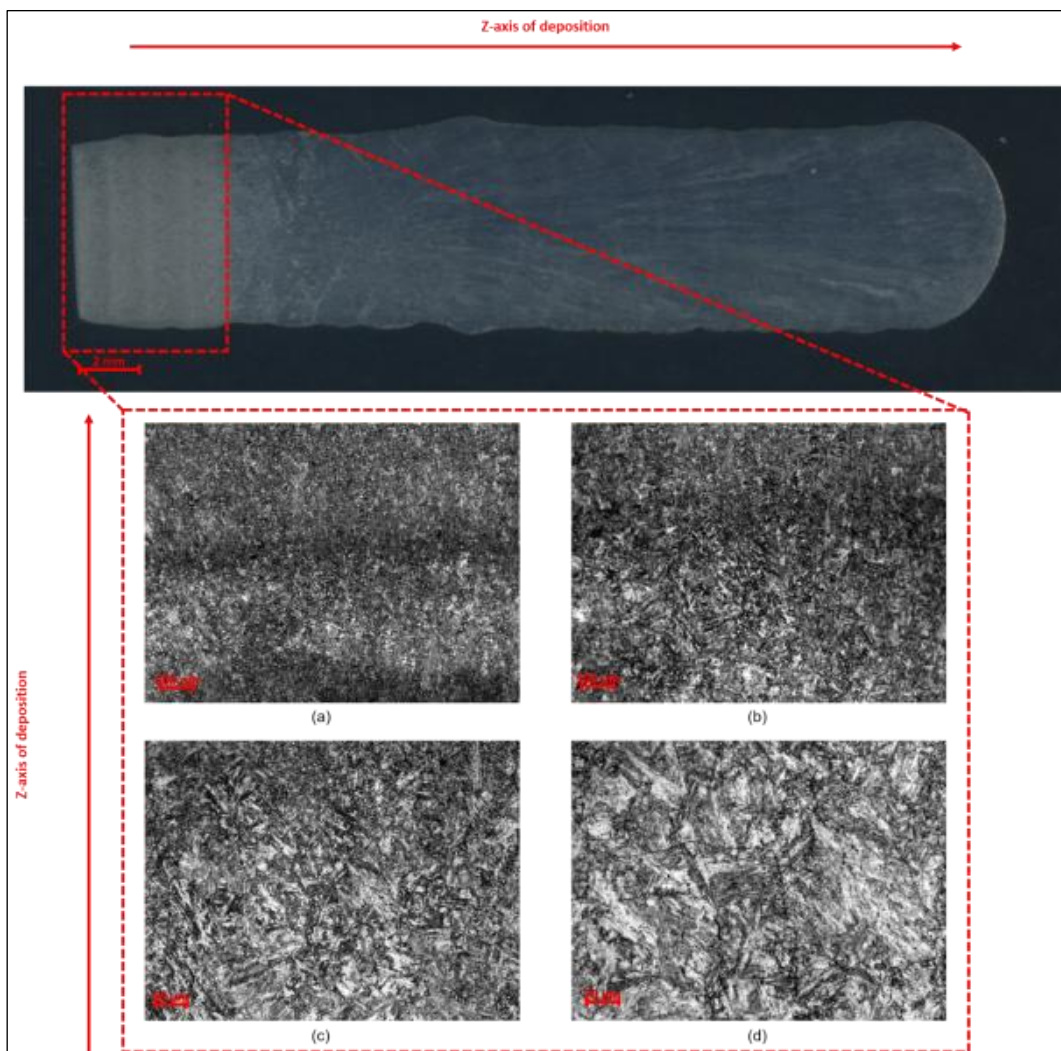


**Fig. 12.** Macro and Microstructure in the bottom portion of the sample

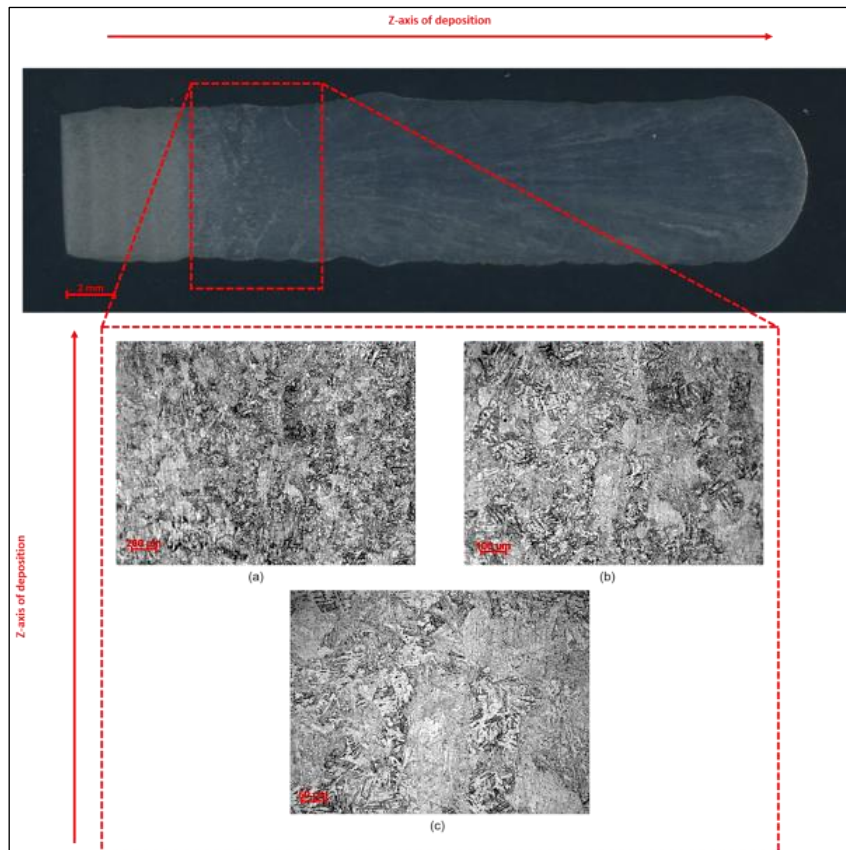


**Fig. 13.** Macro and Microstructure in the middle portion of the sample

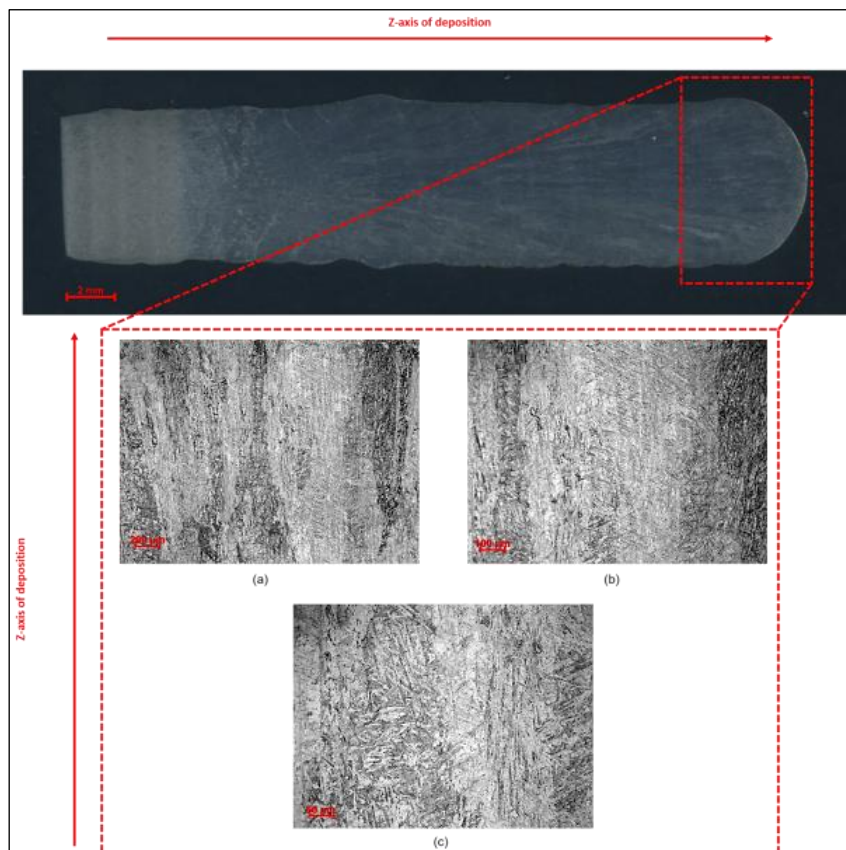


**Fig. 14.** Macro and Microstructure in the top portion of the sample

### 3.6. Tensile Testing

In order to determine the mechanical properties, a layer was deposited using the oscillation path and the CMT parameters similar to the parameters applied for depositing the test artifact, sample O1. As figure 15 shows, two sets of specimens were extracted, one on vertical direction (perpendicular to the deposition direction) and the other on the horizontal direction, (parallel to the deposition direction) to determine the tensile properties. The tensile testing results performed for both the vertical and horizontal specimens are presented in figure. 16a. Specimens V1 to V3 were tested on vertical direction, while samples H1 and H2 on the horizontal. Figure 13b exhibits the true stress-strain curve of specimens V3 and H1. Based on the results processed (Fig. 16), it can be observed that the vertical specimens show higher tensile strength than the horizontal ones (1235 MPa comparing to 1122 MPa), while the latter reveals a significant greater degree of ductility (0.10 vs 0.07). This anisotropy was expected behaviour, and it is justified by the direction of the dendrites relative to the loading orientation [30]. The orientation of dendrites relative to the loading direction has a significant impact on the mechanical

Specimen	YS 0.2% [MPa]	UTS [MPa]	Strain [mm]
V1	970	1226	0.06
V2	941	1235	0.07
V3	949	1224	0.06
H1	887	1092	0.10
H2	842	1122	0.08

a)

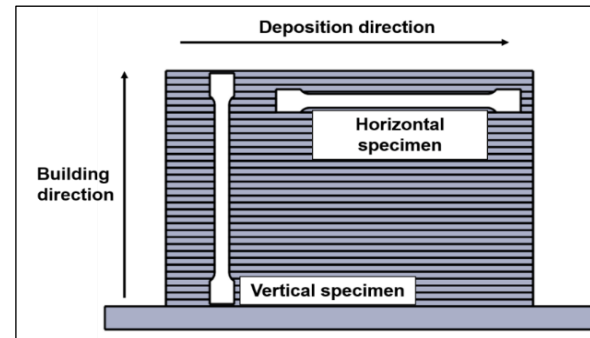
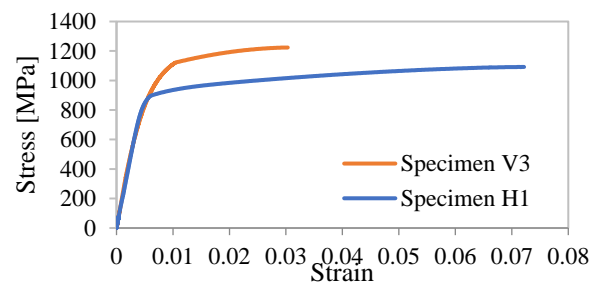


Fig. 15. Orientation of tensile specimens in relation to deposition and building directions [17]



b)

Fig. 16 Tensile testing: a) testing results, b) stress - strain curve of specimens V3 and L1

## 4. CONCLUSIONS

Based on the experimental results, significant conclusions can be drawn, as follows:

- For AISI 410 martensitic stainless-steel deposition with a CMT process, a WFS of 4 m/min with a TS of 0.16 m/min (WFS/TS = 25) should be used as reference to obtain an appropriate bead shape when depositing with a linear path. For an oscillation path, a WFS of 3 m/min with a TS of 0.30 m/min (WFS/TS = 10) should be used as reference.
- Hardness values are 372 HV to 412 HV, which is in agreement with the ones found by Amrei et al. [10] and characteristic of a martensitic structure, which grants parts created with this material high resistance to wear. The hardness values were found to be independent of process parameters.
- For the deposition of the test artifact an oscillation path in both the outer and inner sections provided a better filling of the artifact contour and an

improvement in segment regularity and connectivity, when compared to linear paths.

- Interlayer temperature must be controlled in order to avoid defects between layers. Keeping an interlayer temperature of 200 °C eliminated defects that were present when this control was not enforced.
- Microstructure and macrostructure showed a martensitic structure along the height of the analyzed wall, with grain size getting progressively coarser when approaching the top layer. These results were in alignment with the ones found in a study for a multipass weld of this material [10]. No microstructural defects, such as cracks or lack of fusion, were present in the analysis;
- Tensile testing revealed high values for both UTS and YS in both directions, having UTS values from 1092 MPa to 1235 MPa for, YS from 842 MPa to 970 MPa. It also showed mild ductility for vertical direction with values between 0.06 and 0.07, and significant ductility in the horizontal direction, with values from 0.08 to 0.10.

## ACKNOWLEDGMENTS

This work was supported by the grant ERASMUS+ Strategic Partnership Key Action 2, no: 2021-1-RO01-KA220-VET-000028028, acronym DIGIGREEN, cofinanced by the European Union.

## REFERENCES

- [1] Attaran M., *The rise of 3-D printing: The advantages of additive manufacturing over traditional manufacturing*, Bus. Horiz., Vol. 60 (5), 2017, pp. 677–688, doi: 10.1016/j.bushor.2017.05.011.
- [2] Ding D., Pan Z., Cuiuri D., Li H., *Wire-feed additive manufacturing of metal components: technologies, developments and future interests*, International Journal of Advanced Manufacturing Technology, Vol. 81(1–4), 2015, pp. 465–481, doi: 10.1007/s00170-015-7077-3.
- [3] Williams S. W., Addison A. C., Martina F., Pardal G., Ding J., P. Colegrove, *Wire + Arc Additive Manufacturing*, Materials Science and Technology, Vol. 32(7), 2015, pp. 641–647, doi: 10.1179/1743284715y.0000000073.
- [4] Wang Z., Palmer T. A., Beese A. M., *Effect of processing parameters on microstructure and tensile properties of austenitic stainless steel 304L made by directed energy deposition additive manufacturing*, Acta Materialia, Vol. 110, 2016, pp. 226–235, doi: 10.1016/j.actamat.2016.03.019.
- [5] Yilmaz O., Uglia A. A., *Microstructure characterization of SS308LSi components manufactured by GTAW-based additive manufacturing: shaped metal deposition using pulsed current arc*, International Journal of Advanced Manufacturing Technology, Vol. 89, 2016, pp. 13–25, doi: 10.1007/s00170-016-9053-y.
- [6] Chen X., Li J., Cheng X., He B., Wang H., Huang Z., *Microstructure and mechanical properties of the austenitic stainless steel 316L fabricated by gas metal arc additive manufacturing*, Materials Science and Engineering: A, Vol. 703, Aug. 2017, pp. 567–577, doi: 10.1016/j.msea.2017.05.024.
- [7] Senthil Kumar A., Raja Durai A., Sornakumar T., *The effect of tool wear on tool life of alumina-based ceramic cutting tools while machining hardened martensitic stainless steel*, Journal of Materials Processing Technology, Vol. 173(2), 2006, pp. 151–156, doi: 10.1016/j.jmatprotec.2005.11.012.
- [8] Sequeira Almeida P. M., Williams S., *Innovative process model of Ti-6Al-4V additive layer manufacturing using cold metal transfer (CMT)*, 21st Annual International Solid Freeform Fabrication Symposium - An Additive Manufacturing Conference, SFF 2010.
- [9] Gerhard P., Ferdinand K., Harald C., *Manufacturing of turbine blades by shape giving CMT Welding*, Metal Additive Manufacturing Conference, 2014, pp. 10.
- [10] Amrei M. M., Monajati H., Thibault D., Verreman Y., Germain L., Bocher P., *Microstructure characterization and hardness distribution of 13Cr4Ni multipass weld metal*, Materials Characterization, Vol. 111, 2016, pp. 128–136, doi: 10.1016/j.matchar.2015.11.022.
- [11] Wang T., Zhang Y., Wu Z., Shi C., *Microstructure and properties of die steel fabricated by WAAM using H13 wire*, Vacuum, Vol. 149, 2018, pp. 185–189, doi: 10.1016/j.vacuum.2017.12.034.
- [12] Xu X., Ding J., Ganguly S., Diao C., Williams S., *Oxide accumulation effects on wire + arc layer-by-layer additive manufacture process*, Journal of Materials Processing Technology, Vol. 252, pp. 739–750, October 2017, doi: 10.1016/j.jmatprotec.2017.10.030.
- [13] Martina F., Ding J., Williams S., Caballero A., Pardal G., Quintino L., *Tandem metal inert gas process for high productivity wire arc additive manufacturing in stainless steel*, Additive Manufacturing, Vol. 25, 2019, pp. 545–550 doi: 10.1016/j.addma.2018.11.022.
- [14] Rodrigues T. A., Duarte V., Miranda R. M., Santos T. G., Oliveira J. P., *Current status and perspectives on wire and arc additive manufacturing (WAAM)*, Materials, Vol. 12(7), 2019, doi: 10.3390/ma12071121.
- [15] Zhang Y. M., Chen Y., Li P., Male A. T., *Weld deposition-based rapid prototyping: A preliminary study*, Journal of Materials Processing Technology, Vol. 135(2-3) Spp., 2003, pp. 347–357, doi: 10.1016/S0924-0136(02)00867-1.
- [16] Hu Z., Qin X., Shao T., Liu H., *Understanding and overcoming of abnormality at start and end of the weld bead in additive manufacturing with GMAW*, International Journal of Advanced Manufacturing Technology, Vol. 95(5–8), 2018, pp. 2357–2368, doi: 10.1007/s00170-017-1392-9.
- [17] Suryakumar S., Karunakaran K. P., Bernard A., Chandrasekhar U., Raghavender N., Sharma D., *Weld bead modeling and process optimization in Hybrid Layered Manufacturing*, CAD Computer Aided Design, 2011, doi: 10.1016/j.cad.2011.01.006.
- [18] Xiong J., Zhang G., Hu J., Wu L., *Bead geometry prediction for robotic GMAW-based rapid manufacturing through a neural network and a second-order regression analysis*, Journal of Intelligent Manufacturing, 2014, doi: 10.1007/s10845-012-0682-1.
- [19] Xiong J., Zhang G., Gao H., Wu L., *Modeling of bead section profile and overlapping beads with experimental validation for robotic GMAW-based rapid manufacturing*, Robotics and Computer-Integrated Manufacturing, Vol. 29(2), 2013, pp. 417–423, doi: 10.1016/j.rcim.2012.09.011.
- [20] Xu X., Ding J., Ganguly S., Diao C., Williams S., *Preliminary Investigation of Building Strategies of Maraging Steel Bulk Material Using Wire + Arc Additive Manufacture*, Journal of Materials Engineering and Performance, 2018, pp. 1–7, doi: 10.1007/s11665-018-3521-5.
- [21] Ding D., Pan Z., Cuiuri D., Li H., *A tool-path generation strategy for wire and arc additive manufacturing*, International Journal of Advanced Manufacturing Technology, Vol. 73(1–4), 2014, pp. 173–183, doi: 10.1007/s00170-014-5808-5.
- [22] Kao J., Prinz F. B., *Optimal Motion Planning for Deposition in Layered Manufacturing*, ASME Design Engineering Technical Conferences., Atlanta, Georgia, September 13–16 1998, pp. 10.
- [23] Ayarkwa K. F., Williams S., Ding J., *Investigation of pulse advance cold metal transfer on aluminium wire arc additive manufacturing*, International Journal of Rapid Manufacturing, Vol. 5(1), 2015, pp. 44, doi: 10.1504/ijrapidm.2015.073547.
- [24] Lockett H., Ding J., Williams S., Martina F., *Design for wire + Arc additive manufacture: Design rules and build orientation selection*, Journal of Engineering Design, Vol. 28(7–9), 2017, pp. 568–598, doi: 10.1080/09544828.2017.1365826.
- [25] Mehnen J., Ding J., Lockett H., Kazanas P., *Design study for wire and arc additive manufacture*, International Journal of Product Development, Vol. 19(1–3), 2014, pp. 2–20, doi: 10.1504/IJPD.2014.060028.
- [26] Venturini G., Montevocchi F., Scippa A., Campatelli G., *Optimization of WAAM Deposition Patterns for T-crossing Features*, Procedia CIRP, Vol. 55, 2016, pp. 95–100, doi: 10.1016/j.procir.2016.08.043.
- [27] Wu B., Ding D., Pan Z., Cuiuri D., Li H., Han J., Fei Z., *Effects of heat accumulation on the arc characteristics and metal transfer behavior in Wire Arc Additive Manufacturing of Ti6Al4V*, Journal of Materials Processing Technology, Vol. 250, 2017, pp. 304–312, doi: 10.1016/j.jmatprotec.2017.07.037.
- [28] Rios S., Colegrove P. A., Martina F., Williams S., *Analytical process model for wire + arc additive manufacturing*, Additive Manufacturing, Vol. 21, 2018, pp. 651–657, doi: 10.1016/j.addma.2018.04.003.
- [29] Divya M., Das C. R., Ramasubbu V., Albert S. K., Bhaduri A. K., *Improving 410NiMo weld metal toughness by PWHT*, Journal of Materials Processing Technology, Vol. 211(12), 2011, pp. 2032–2038, doi: 10.1016/j.jmatprotec.2011.06.024.
- [30] Pragana J. P. M., Cristino V. A. M., Bragança I. M. F., Silva C. M. A., Martins P. A. F., *Integration of Forming Operations on Hybrid Additive Manufacturing Systems Based on Fusion Welding*, International Journal of Precision Engineering and Manufacturing-Green Technology, Vol. 7, 2020, pp. 595–607, doi: 10.1007/s40684-019-00152-y.